QIRT'2022

10.21611/qirt.2022.2025

16th Quantitative InfraRed Thermography Conference

Numerical and Experimental investigations of pulsed infrared Thermography for damage detection in Honeycomb Sandwich Composites

by S. Unnikrishnakurup*, J. Zheng*, C. Manzano*, C. Y. Ngo*

* *Structural Materials Department, Institute of Materials Research and Engineering(IMRE), A*STAR, Singapore*

Abstract

This paper investigates the inspection and testing of internal structural damages in Honeycomb Sandwich composites by means of pulsed thermography experiments. The voids, delamination flaws, and epoxy-filled defects are also studied using numerical simulation in 3D FEM using COMSOL Multiphysics. Pulse thermography data processing methods such as Thermographic Signal Reconstruction (TSR) techniques, Pulse Phase Thermography (PPT) and Principle Component Analysis (PCA) were used to analyse the simulated and experimental data. Standard samples made of Nomex and fiber glass cores, both of which had identical flaws, were studied. The potted core defect, filled with epoxy, and the pillow insert (delamination) located in the front face plate of the composite could be clearly identified from the thermograms as well as the TSR results. On the contrary, the machined core defects showed very minute contrast and are more difficult to be identified.

1. Introduction

Due to honeycomb composite's great strength, low weight, and longevity, they are frequently employed in the production of airplane structures and components. [1]. Honeycomb structures come in a variety of shapes and sizes, but they always have the same basic features. A uniform two-dimensional array of hollow cells is formed between two thin vertical walls that are bonded with adhesive in honeycomb structures that provides strength in tension. Newer honeycomb structures with a low density and high out-of-plane compression and shear capabilities have been developed. One disadvantage of this type of composite sandwich structures is that it is extremely vulnerable to damage, which can occur because of object's impacts during flights, stress undergone by the composite parts due to thermal cycling, among other reasons. Some of the most significant defects in honeycomb structures are delamination in the fiber reinforced polymer face plates, excessive adhesive material and damaged honeycomb inner core [2].

The use of thermal technologies for nondestructive assessment (NDE) of composite sandwich structures is gaining popularity. Infrared Thermography has a number of advantages, including being non-contact, quick, capable of imaging large areas, adaptable to complicated geometries, and quantitative. When only a small quantity of heat is delivered to the structure's surface, the procedure is safe. Thermography has demonstrated to be an effective tool for detecting faults in composite structures. Face sheet delaminations, face sheet to core disbonds, and core crushing are defects of interest in composite honeycomb systems. Active Thermography is a viable non-destructive inspection method for routine evaluation of large area aircraft honeycomb sandwich panels to detect such problems [3]. Because the composite face sheets are often thin in comparison to the total thickness, thermography is an useful method for detecting face sheet delaminations. It's crucial to detect face sheet to core disbonds. Face sheet to core disbonds can increase under stress, resulting in disbond buckling failure and catastrophic structural failure. Core potting is a great approach to make a reference standard that may be used to depict splices or honeycomb repair.

Honeycomb specimens with artificial faults were utilized in this study to evaluate the efficacy of pulsed thermography examination together with a 3D numerical model devised to replicate the experimental approach. Various post-processing techniques have been applied to analyze and interpret the data such as Thermographic Signal Reconstruction (TSR), Principle component Analysis (PCA) and Pulse Phase Thermography (PPT). The pulsed thermography thermal results have been processed using TSR, PPT and PCA based thermography data processing algorithms and compared.

2. Materials and Methods

The Honeycomb sandwich sample investigated in this study consists of three embedded engineered flaws which simulate structural defects commonly found in honeycomb components. Those defects were made during the fabrication of the honeycomb sample. The composite panel used in this study is $30.4X27.9cm$ and thickness is 1 mm. The sample was constructed with two equally sized honeycomb cores of cell height 25.4 mm, one made of Nomex and the other one made of fiberglass placed next to each other making up the sample's central core sandwiched in between 6 plies of plain weave prepreg carbon fiber sheet cloth $[+45, 90, -45]_2$ as shown in Figure 1.

Three types of defects were made, see Figure 2: 1. A potted core of 25.4 mm diameter, 2. Pillow insert of diameter 25.4 mm in the carbon fiber face plate after 4th layer, and 3. A machined core of diameter 25.4 mm. Potted core defects are manufactured by completely removing the core material to create through holes and refilling them with epoxy resin. The flaws are located only on one side of the composite honeycomb panel. Pillow inserts are made by placing Kapton and paper tissue

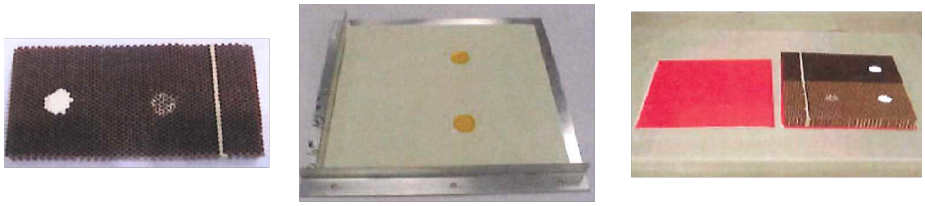

(a) (b) (c)

Fig. 1. ***Honeycomb Sample with engineered defects (a) Honeycomb core showing potted core, machined core and core splice areas (b) Composite plied being laid up with pillow insert delamination flaws (c) Adhesive layer placed on flawed laminate with both cores in place on lower laminate skin***

layered in between carbon fiber sheets. Machined core defects, acting as void defects, were made by partially milling out the honeycomb cores creating air filled volumes encapsulated by the composite core and carbon fiber layers of the sample's front face plate. A commercially available thermal inspection system was used to collect thermographic single side flash inspection data. The power supply giving 6 kJ of energy to the flash tubes provide the flash power. The flash duration is 2.5 milliseconds and is instantaneous compared to the frame rate of the camera (100 frames per second) and the thermal response time of the composites.

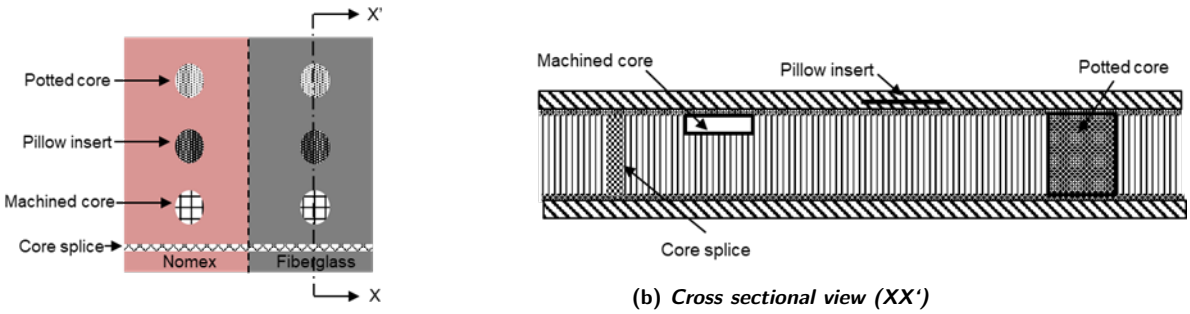

(a) ***plan view*** **(b)** ***Cross sectional view (XX')***

Fig. 2. ***Schematic of the top view and cross sectional view of honeycomb panel with engineered defects***

2.1 Post-processing methods

The most often used methods for post-processing thermographic raw data are based on the assumption that there is very little heat transfer in the lateral direction once the sample surface has been excited. Based on this assumption, the heat conduction equation in material may be simplified as follows.

$$\frac{\partial^2 T}{\partial x^2} = \frac{1}{\alpha}\frac{dT}{dt} \tag{1}$$

Where T is the temprature and α is the diffusivity. The solution of this 1 dimensional heat equation for a semi-infinite body under instantaneous pulse energy can be derived as follows

$$T(x,t) = \frac{Q}{e\sqrt{\pi t}} e^{-\frac{x^2}{4\alpha t}} \tag{2}$$

Where Q is is the absorbed energy per surface area, $e = \sqrt{k\rho c}$ is the thermal effucivity, x is the depth and t is time. The surface temperature can obtained from this expression for x=0 and is given as

$$T(t) = T(0,t) = \frac{Q}{e\sqrt{\pi t}} \tag{3}$$

Thermographic Signal Reconstruction (TSR) [4] method is used to analyse the experimental time dependant temperature profiles. The approach applies a smoothing function to fit the raw log-log data and then uses the replica for additional

processing. A transform can be constructed and saved once the equations of fit have been placed in the log domain. The first and second derivatives are now the most useful functions. Because this method produces considerable increases in noise reduction, the TSR approach has been used to identify smaller and deeper faults. The Fourier Transform (FT) is another important technique in pulse thermography [5]. The thermal images are transformed from the time domain to the frequency domain in FT mode, or Pulse phase thermography (PPT), by employing Discrete Fourier Transform (DFT) to handle temperature fluctuations. A fast Fourier transform was used to compute phase. The FT considerably minimized effects of the non-uniform heating. Principal Component Analysis (PCA) is a common post-processing technique for thermal image sequences [6, 7]. Principle component analysis (PCA) approach involves the application of singular value decomposition.

3. Numerical Simulation

The 3D FEM simulations were carried out in COMSOL MULTIPHYSICS software to investigate the heat transport through the honeycomb sandwich. All of the composite sample's components are included in the simulations, including the face plate, honeycomb core, and all three types of defects, such as potted core, pillow insert, and machined core. The sliced core is not modelled in this study. To reduce the model size, a reduced scale geometry is modelled as shown in figure 3a. The face plate and a portion of the honeycomb is modelled with a symmetry boundary condition at the free end of the honeycomb core. The face plate size is $24 \times 16 \times 1mm^3$, adhesive layer of thickness of $0.2mm$ and core thickness of $2mm$. The pillow insert (delamination) in the face plate is modelled as a thin thermally resistive layer [8] of 0.3 mm thickness which is placed $0.75mm$ from the boundary between adhesive layer and the face plate. The lateral dimensions of all the defects are set as 2 mm diameter. Figure 3b shows the meshed geometry. The thermal properties of the materials used in the simulation are listed in Table 1.

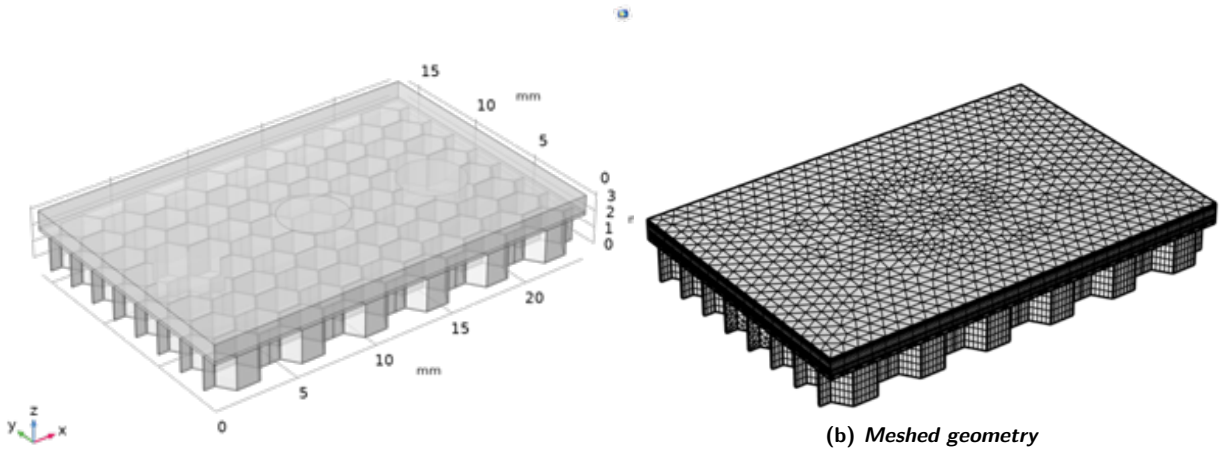

(a) ***FEM Geometry***

(b) ***Meshed geometry***

Fig. 3. ***FEM Model***

Table 1. *Thermal properties of materials [9]*

Material	Thermal Conductivity	Specific heat	Density
CFRP	0.61	1758	1500
Epoxy Adhesive	0.18	1100	1200
Pillow Insert (Kapton tape)	0.12	1172	2170
Nomex Honeycomb	0.14	1100	1000

The maximum value of heat flux density applied on the top skin surface is $2 \times 10^6\ W/m^2$. The flash duration is $2.5ms$ and the model is run for 10 s. During the heat flux application, a very fine time step ($1 \times 10^{-5}s$) is employed, and as the thermal gradient across the thickness lowers, a progressively rising time step is used at different time intervals. Figure 4 shows the temperature distribution at the end of flash heating (t = 10 s)

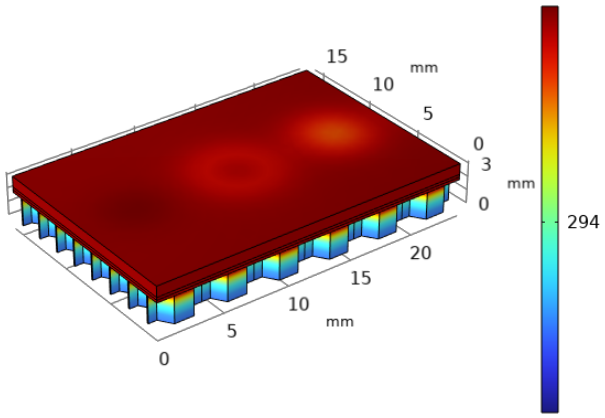

Fig. 4. ***Simulation result: Surface temperature at the end of flash heating (t=10 s)***

4. Results and Discussion

4.1 Absolute contrast analysis

The trends related to the heating characteristics of experiments are eliminated using data processing approaches [10]. The findings of the temperature-time profile from experiment are plotted on a log-log scale in Figure 5(a). The temperature decay is linear initially prior and just immediately after the flash excitation. The after glow effect due to the radiation from the lamp after the flash excitation [11] also caused initial nonlinear behaviour in the experimental results. The linear behaviour changes as the heat diffuses into the material and interact with the defects' heterostructures boundaries. The temperature decay in the case of the pillow insert slows down as it encounters the heat flow first. The temperature decay in the sound zone and machined core region changes as the heat flow reaches the face plate thickness and then the adhesive layer. Because the thermal effusivity of epoxy is greater than that of air, the temperature degradation in a potted core continues. Figure 5b shows the absolute contrast of the defective region with respect to the sound region. The reference sound region is selected around the respective defective area.

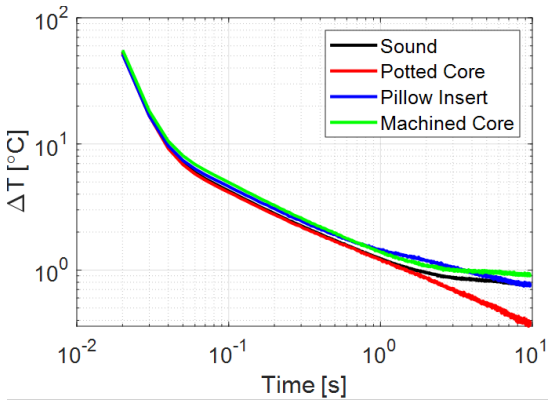

(a) ***Temperature-time plot***

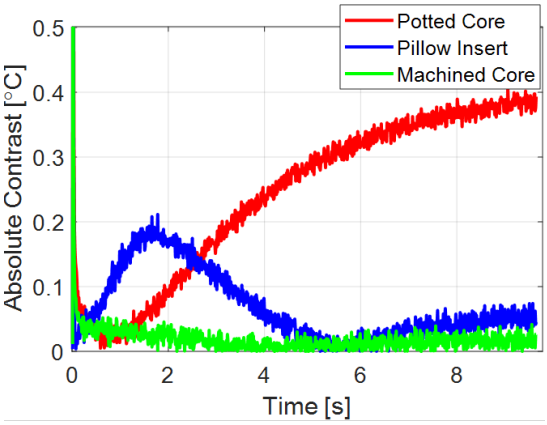

(b) ***Absolute contrast***

Fig. 5. ***Experimental results***

Figure 6a and 6b shows the temperature-time profile and the absolute contrast respectively from simulation. The trend of the simulated findings matches that of the experiment. The cooling rate in the potted core region of the experiment was not stabilized at the end of the experiment (10 s), although the simulation attained steady state. This is to be anticipated, as the simulation was run on a smaller model with a potted core region of just 2 mm, but in reality, the epoxy filling in the sample is spread throughout the whole honeycomb thickness of 25.4 mm. The pillow insert is modeled as a 0.3 mm thick thermally resistive layer (0.2 mm thick tissue paper held between two layers of 0.05 mm thick kapton tape, situated just after the 4th ply from the top of the CFRP face sheet) with the same material properties as the kapton tape. Due to differences in material

characteristics of the kapton tape and paper combination, the cooling rate in this location is not accurately represented. In the contrast plot, the machined core defect, which corresponds to the disbond between the core and the adhesive region, displays a very little contrast with the noise level. The findings of the simulation might potentially demonstrate a progressive increase in contrast over time.

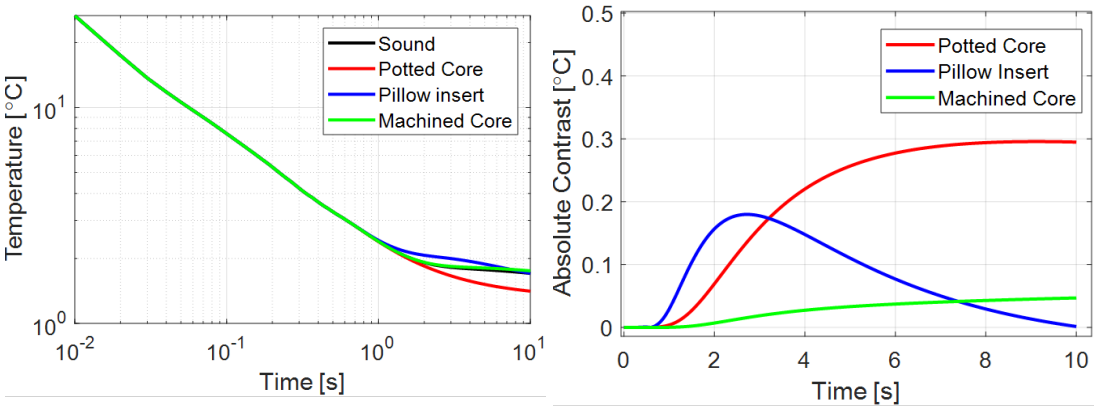

(a) ***Temperature-time plot*** **(b)** ***Absolute contrast***

Fig. 6. ***Simulation results***

Figure 7 presents the comparison of thermal contrast for different defects between the Nomex and fiber glass core honeycomb regions. The temperature contrast trends are the same in both cases. Since we only employed one flash lamp in this investigation, which was placed in front of the sample near the Nomex core region, there is a non-uniform heating effect on the sample surface, which causes the contrast values to vary.

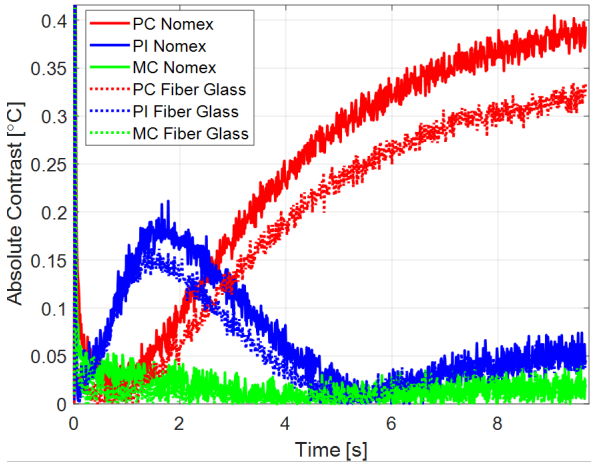

Fig. 7. ***Comparison of absolute contrast for Nomex and fiber glass core defects***

4.2 Thermographic Signal Reconstruction

The temperature-time data, as given by 3, is converted to a logarithmic scale, which results in a linear relation between time and temperature with a slope of $1/2$ and is given by

$$ln(\Delta T(t)) = ln(\frac{Q}{e}) - \frac{1}{2}ln(\pi t) \tag{4}$$

As a result of many factors such as nonlinear phase response and background radiation, the temperature response curve is disturbed, and does not meet the linear relation in an ideal manner. Hence, the logarithmic temperature progress may be represented by an n-degree polynomial function.

$$ln(\Delta T(t)) = a_0 + a_1 ln(\pi t) + a_2[ln(\pi t)]^2 + ... + a_n[ln(\pi t)]^n \tag{5}$$

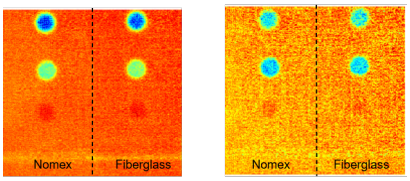

Fig. 8. ***TSR first and second derivative images***

4.3 Pulse phase thermography analysis

Pixel by pixel analysis will be performed on a thermographic image sequence consisting of N images captured during a total time T. The time signal transformation into the frequency domain is by a discrete Fourier Transform [12] and is given by:

$$F_n = \sum_{k=0}^{N-1} T_k e^{-2\pi i k n/N} = Re_n + Im_n \tag{6}$$

From the real and imaginary parts of the transform result for the frequency number n,Re_n and Im_n, respectively, the amplitude A_n and the phase ϕ_n can be calculated

$$A_n = \sqrt{Re_n^2 + Im_n^2} \tag{7}$$

$$\phi_n = arctan\frac{Im_n}{Re_n} \tag{8}$$

Here n is index of frequency(n=0,1,...(N-1)). For discrete, evenly spaced frequencies, an amplitude and phase image are created after execution for all pixels.

$$f_n = \frac{n}{T} \tag{9}$$

In order to considerably speed up the computation for all pixels of an image, equation 6 is usually performed using a fast Fourier transform (FFT) technique. The computational burden is in the N log N range. Figure 9 presents the pulse phase thermography results. The phase information with frequency for all the three defective region and the non-defective (sound) region in the nomex core honeycomb is plotted in figure 9(a). The phase contrast is then calculated by taking difference in phase between the defective region and the sound region and are plotted in figure 9(b). Similarly the phase and the phase contrast for the glass fiber core honey comb is plotted in figure 9 (c) and (d) respectively. It is identified from this analysis that the maximum phase contrast is occurring at frequency f=0.0518 Hz. The phase image corresponding to this frequency is shown in figure 9(e). A line profile is drawn across the defective region in both nomex core and the fiber glass core honeycomb are presented in figure 9(f) and (g) respectively. The signal for both the potted core defect and the pillow insert is extremely good, while the signal for the machined core defect is very faint in both cases.

4.4 Principal component analysis

This algorithm is based on decomposition of the thermal data into its principal components or eigenvectors. The PCA is calculated by constructing a data matrix A in which temporal variations are represented by columns and spatial image pixel locations are represented by rows. By removing the mean along the time dimension, the matrix A is modified. Singular value decomposition may then be used to decompose matrix A as follows:

$$A^T A = U * \Gamma^2 * U^T \tag{10}$$

Where Γ is a diagonal matrix. The eigenvectors may be found in the U columns. Pixel by pixel, the PCA image is created by multiplying the selected eigenvector times the temperature response (data matrix A). Figure 10 shows the first five empirical orthogonal functions.

4.5 Post-processing methods comparison

Figure 11(a) to (d) presents the comparison of all the thermographic post-processing results on the experimental thermal images. All post-processing techniques successfully detected the potted core flaw and the pillow insert with good contrast. The crushed core defect contrast is very minute in comparison to the other two defects and the shape of the defect is not fully represented compared to the ultrasonic C-scan results as hon in figure 11(e).

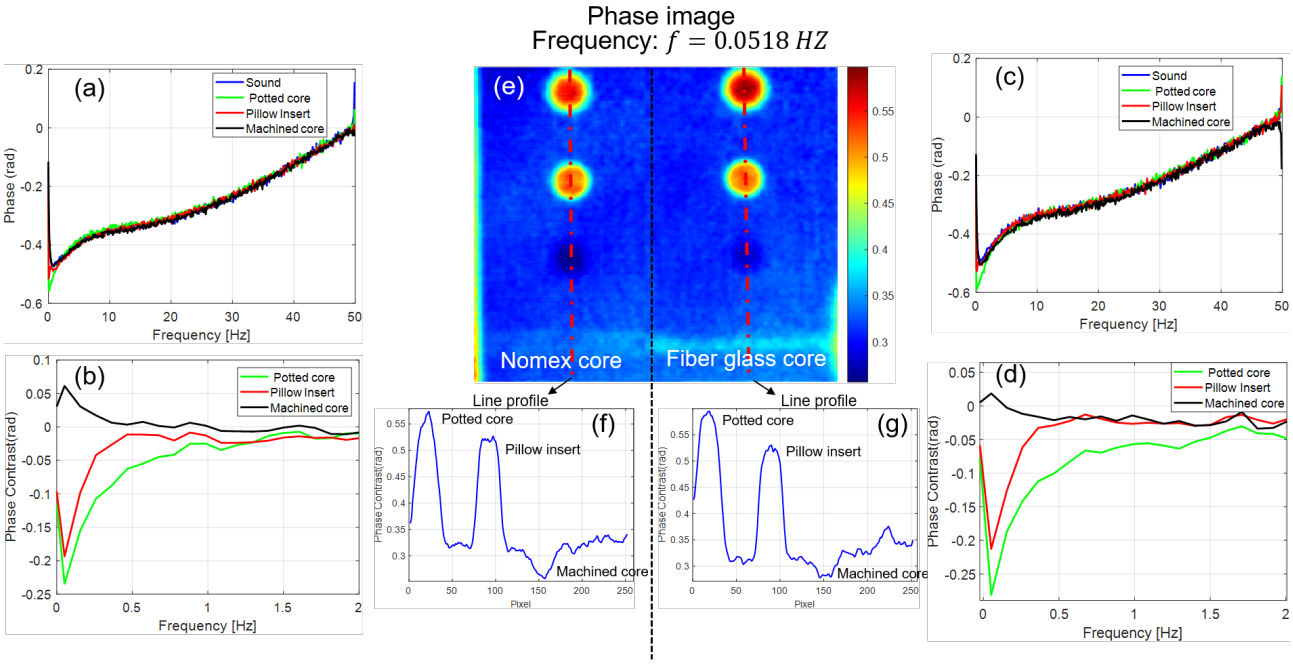

Fig. 9. ***Pulse Phase Thermography Results (a) Phase plot Nomex core honeycomb (b) Phase contrast plot Nomex core honeycomb (c) Phase plot glass fiber core honeycomb (d) Phase contrast glass fiber core honeycomb (e) PPT phase image at frequency 0.0518Hz (f) Line profile across defective region: Nomex core honeycomb (g) Line profile across defective region: fiber glass core honeycomb***

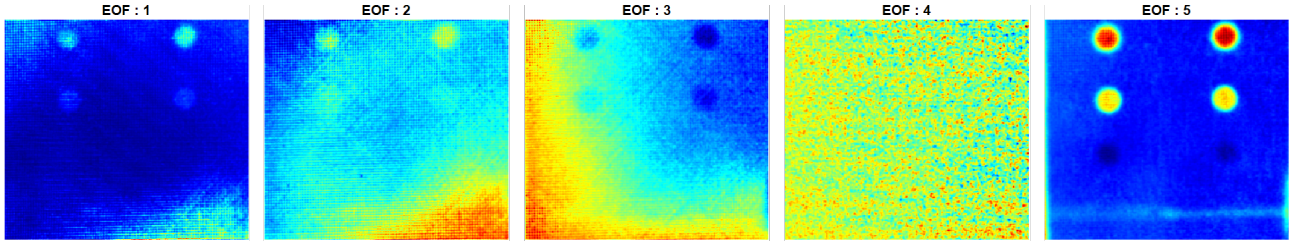

Fig. 10. ***PCA Results: First 5 empirical orthogonal functions (EOF)***

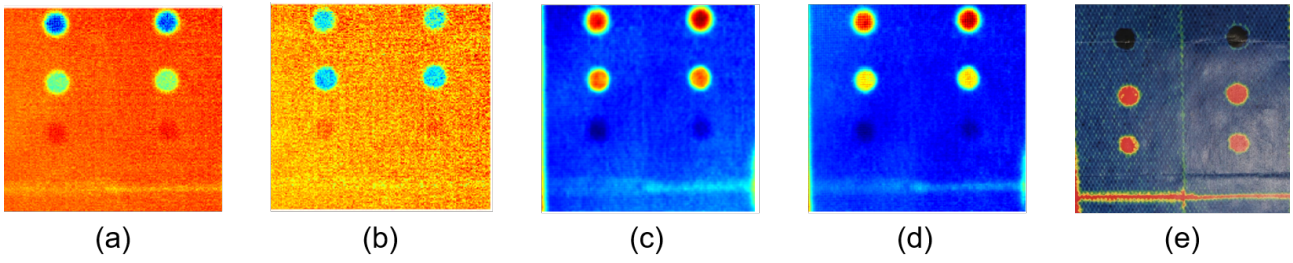

Fig. 11. ***Honeycomb Sample with engineered defects (a) TSR first derivative (b) TSR second derivative (c) PPT phase image at frequency 0.0518Hz (d) PCA at EOF 5 (e) Ultrasonic C-Scan***

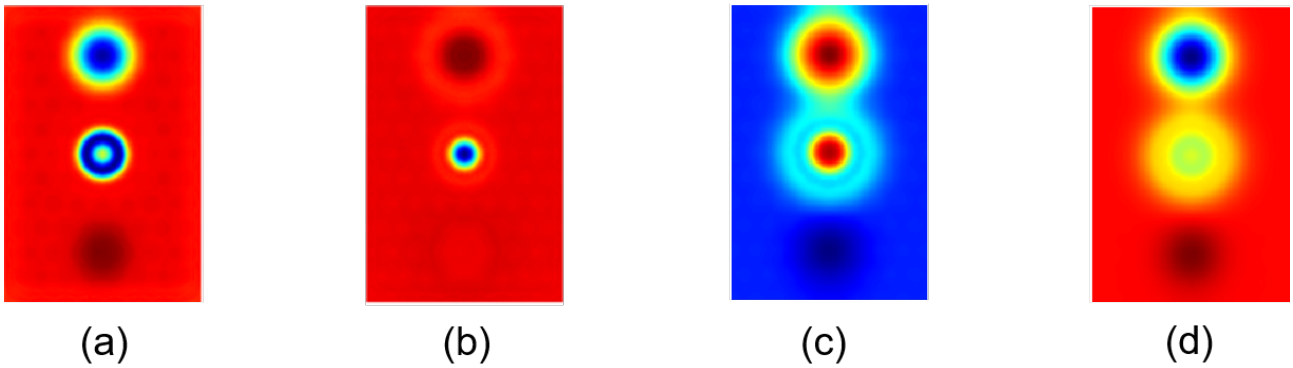

Fig. 12. ***Post-processing results on Simulation data (a) TSR first derivative (b) TSR second derivative (c) PPT phase image at frequency 0.0518Hz (d) PCA at EOF 5 (e) Ultrasonic C-Scan***

4.6 SNR comparison

Figure 13 shows the cumulative sum method used to evaluate the SNR values from raw thermogram and different post-processing results.As illustrated in figure 13(a), this procedure begins by selecting a contrast region that includes both sound and defect areas. Figure 13(b) also shows the values from this area sorted and plotted. The signal value in a raw thermogram is defined as the deference between temperature values more than $0.9 \times (Tmax - Tmin)$ and temperatures less than $0.1 \times (Tmax - Tmin)$. The standard deviation (STD) of temperatures from a larger reference area is defined as the noise.

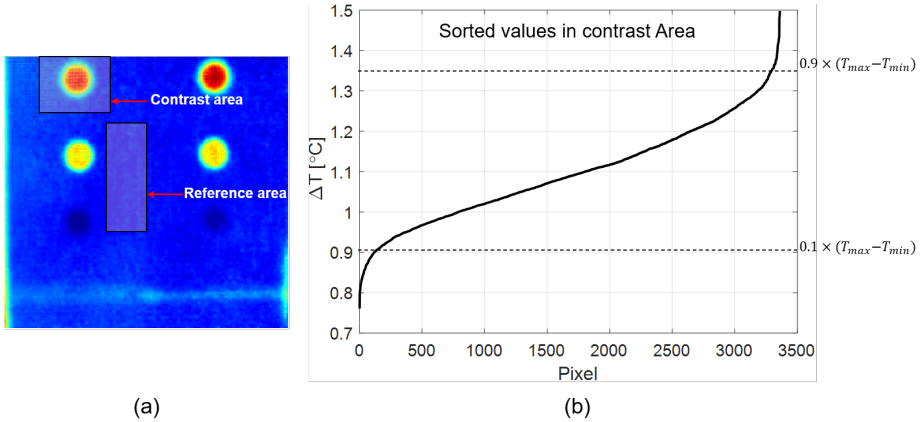

Fig. 13. ***Cumulative sum method to calculate SNR***

The SNR is defines as:

$$SNR = \frac{T_d - T_s}{STD(T_{ref})} \tag{11}$$

where T_d, T_s and T_{ref} are temperature values from defect, sound and reference locations respectively and STD is the standard deviation operation.

The SNR comparison for different thermographic post-processing approaches compared to the raw thermogram is shown as radar plot in Figure 14 (a) and (b) for Nomex and fiber glass honeycomb core, respectively.For all three defect scenarios, the raw thermogram exhibits the lowest SNR. The maximum SNR for potted core defect was obtained using PCA post-processing, which was 36.65 dB and 64.19 dB for Nomex and fiber glass core honeycomb, respectively. Using the PCA approach, the highest SNR for pillow insert defect was 45 dB for nomex and 55 dB for fiber glass core honeycomb.

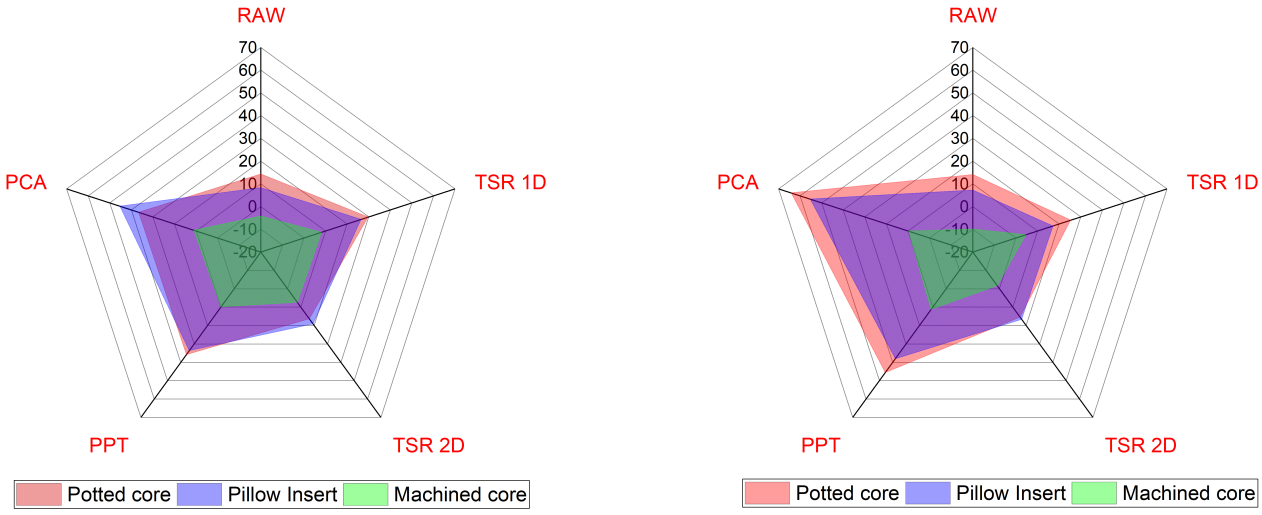

(a) ***Nomex core*** **(b)** ***Fiber Glass core***

Fig. 14. ***SNR(dB) comparison for different thermographic post-processing methods***

5. Conclusion and Summary

This study investigates the temperature signal signature on the skin surface of a carbon fiber composite honeycomb sandwich structure in pulsed thermography reflection mode utilizing numerical modeling and experiment. Three types of defects are planted in the honeycomb structure below the test surface. They are all tested using pulsed thermography, and the thermal sequence and intensity graph obtained by this method are analyzed. The numerical model accurately represented the temperature response of the manufactured flaws. Thermographic signal processing techniques were employed on both experimental and simulated data, and the results were compared qualitatively to ultrasonic C-scan results. The results show that pulsed thermography is an effective nondestructive technique for inspecting delamination in face sheet, and disbonding defects, and it can precisely distinguish the location and dimension of the defect.

Acknowledgements

This research work was supported by the Agency for Science, Technology and Research (A*STAR) through grants under its Singapore Aerospace Programme Cycle 15 (Grant No. M2115a0093 and M2115a0094) and Polymer Matrix Composites Programme (Grant No. A19C9a0044).

References

[1] Hossein Towsyfyan, Ander Biguri, Richard Boardman, and Thomas Blumensath. Successes and challenges in non-destructive testing of aircraft composite structures. *Chinese Journal of Aeronautics*, 33(3):771–791, 2020.

[2] David Glenn Moore and Ciji L Nelson. Damage assessment of composite honeycomb material using advanced inspection technologies. Technical report, Sandia National Lab.(SNL-NM), Albuquerque, NM (United States), 2012.

[3] Huijuan Li. Investigation of honeycomb structure using pulse infrared thermography method. In *Infrared, Millimeter Wave, and Terahertz Technologies*, volume 7854, pages 332–336. SPIE, 2010.

[4] Steven M Shepard. Temporal noise reduction, compression and analysis of thermographic image data sequences, February 4 2003. US Patent 6,516,084.

[5] Xavier Maldague, François Galmiche, and Adel Ziadi. Advances in pulsed phase thermography. *Infrared physics & technology*, 43(3-5):175–181, 2002.

[6] Nikolas Rajic. Principal component thermography for flaw contrast enhancement and flaw depth characterisation in composite structures. *Composite structures*, 58(4):521–528, 2002.

[7] K Elliott Cramer and William P Winfree. Fixed eigenvector analysis of thermographic nde data. In *Thermosense: Thermal Infrared Applications XXXIII*, volume 8013, pages 225–235. SPIE, 2011.

[8] Christiane Maierhofer, Rainer Krankenhagen, Mathias Röllig, Sreedhar Unnikrishnakurup, Christian Monte, Albert Adibekyan, Berndt Gutschwager, Lenka Knazowicka, Ales Blahut, Mike Gower, et al. Influence of thermal and optical material properties on the characterization of defects in fiber composites with active thermography methods. *tm-technical measuring*, 85(1):13–27, 2018.

[9] Vladimir P Vavilov, Y Pan, AI Moskovchenko, and Alexander Čapka. Modelling, detecting and evaluating water ingress in aviation honeycomb panels. *Quantitative InfraRed Thermography Journal*, 14(2):206–217, 2017.

[10] Barbara Szymanik, Sreedhar Unnikrishnakurup, and Krishnan Balasubramaniam. Background removal methods in thermographic non destructive testing of composite materials. *The e-Journal of Nondestructive Testing*, 20(6), 2015.

[11] Christiane Maierhofer, Philipp Myrach, Mercedes Reischel, Henrik Steinfurth, Mathias Röllig, and Matthias Kunert. Characterizing damage in cfrp structures using flash thermography in reflection and transmission configurations. *Composites Part B: Engineering*, 57:35–46, 2014.

[12] Xavier Maldague and Sergio Marinetti. Pulse phase infrared thermography. *Journal of applied physics*, 79(5):2694–2698, 1996.